Energy Science & Engineering

Open Access

MODELING AND ANALYSIS

Robust control design for air breathing proton exchange membrane fuel cell system via variable gain second-order sliding mode

Naghmeh Mirrashid[1], Seyed Mehdi Rakhtala[2] & Mahmood Ghanbari

[1]Faculty of Engineering, Department of Electrical Engineering, Azad Aliabad University, Aliabad-e Katul, Iran
[2]Faculty of Engineering, Department of Electrical Engineering, Golestan University, Gorgan, Iran

Keywords
Lyapunov stability, oxygen excess ratio, PEM fuel cell, second-order sliding mode, variable gain super twisting algorithm

Correspondence
Seyed Mehdi Rakhtala, Faculty of Engineering, Department of Electrical Engineering, Golestan University, Gorgan-Alghadir Blvd- 4918888369, Iran.
E-mail: sm.rakhtala@gu.ac.ir

Funding Information
No funding information provided.

Received: 1 December 2017; Revised: 17 March 2018; Accepted: 3 May 2018

***Energy Science & Engineering* 2018; 6(3): 126–143**

doi: 10.1002/ese3.199

Abstract

The nonlinear and time-dependent characteristic and unknown modeling uncertainty of proton exchange membrane fuel cell (PEMFC) such as complex electrochemical, thermal, and fluid mechanic phenomena make its controller design quite challenging. In this paper, a controller based on a super twisting algorithm (STA) with variable gains is proposed to control the air breathing system of PEMFC. The strategy includes regulating the oxygen excess ratio (λ_{O_2}) for preventing the stack oxygen starvation and maintaining optimum net power output in spite of external disturbances and model uncertainties. The proposed algorithm has the main advantages of the fixed gain STA, such as robustness against the disturbance and parametric uncertainties with the unknown boundary, chattering reduction, and finite time convergence. The Lyapunov analysis was proposed to assess the stability of the Variable Gain Super Twisting Algorithm (VGSTA). The results verified the effectiveness of the proposed controller with attaining robust regulation against uncertainties, disturbances, and noisy circumstance compared to fixed gain SOSM controllers.

Introduction

Fuel cells are as a good alternative source to its high autonomy for the distributed generation power system, electric vehicles. This is due to high-efficiency, renewable, lower gas emissions, low environmental pollution, and consumption of fuels (methanol, hydrogen, solid oxide, etc.) [1, 2]. Furthermore, they have been studied in many power applications as stand-alone power generations [3] and in transportation (cars, buses) [4] due to the high-efficiency and less greenhouse-gas emissions compared to fossil fuels [5].

A main issue in PEM fuel cell operation is the oxygen starvation phenomenon that happens during sudden increasing of load variations. The rapid load rising accelerates the oxygen consumption because of increasing of the chemical reactions in PEMFC that causes irreversible damage as a hot spot on the membrane [5–7]. Load change (I_{st}) as a measurable disturbance causes a severe decrease in λ_{O_2} and strongly affects system operation. The λ_{O_2} requires to be kept between 2 and 2.5 [8] to avoid oxygen starvation, which needs accurate control of the air breathing system.

The air breathing system of the PEMFC connected to a motor and air compressor via a cathode supply manifold. Therefore, its efficiency has a high effect upon the overall dynamic efficiency and transient behavior of the fuel cell under load variation [9]. Thus, new advanced compressor control is essential to improve the performance of the PEMFC system and is a challenging control target. In the recent years, many control strategies have been proposed for adjusting the oxygen excess ratio and maximizing the output net power. A second-order sliding mode algorithm is developed for the PEM fuel cell air feed system. The oxygen excess ratio is estimated via an extended state observer from the measurements of the compressor flow rate, the load current, and the supply manifold pressure. The proposed extended state observer-based controller is

an out feedback system. This out feedback system has robustness against load variations and parametric uncertainties [10]. However, implementation of this control approach is so complex calculation and computing. In Ref. [11], theory of sliding mode control for uncertain stochastic systems and state observer designing to estimate the system state and the stochastic stability for the overall closed-loop system is analyzed. Among them, Purkrushpan and coworkers proposed a feedback control using Jacobin linearization at the nominal operating point. However, a drawback to the system is that the parametric uncertainties, the system severe nonlinearity and large disturbances; linearization control techniques cannot easily satisfy dynamic performance [8]. Niknezhadi and Fantova suggested a LQR/LQG method for adjusting of oxygen stoichiometry [12]. The LQR/LQG method is based on a linearized model at working point using its first derivative (Jacobin matrix) of the Taylor series. Even so, in that study, classic control approaches and the linear control strategy need to find precise knowledge of the model at operating point. Another drawback with this system is that finding exact model; it is impossible and so difficult when the system is a very complex and transient response is unsuitable and there is a steady-state error for tracking. Therefore, an advanced control technique requires to be developed based on the nonlinear dynamic model for the PEMFC.

Na et al. [8, 13] used an advanced controller based on the exact nonlinear model. The results from this research indicated that the suggested feedback linearization controller had a better transient response. Although the problem is that the feedback linearization controller could not assure the robustness with the parametric uncertainties and the internal and external disturbances. Another issue is the requirement of an exact nonlinear model to design a controller. To solve this issue, Li et al. [14] designed a robust control strategy based on H∞ and the state feedback exact linearization. So, the steady-state error is alleviated against parameter uncertainty, and the system robustness and better transient response are guaranteed. However, the drawback in this method is that this control approach has some complex mathematical calculation, and the calculation is very time-consuming and hard to implementation.

The intelligent, low-cost, and nonlinear controller is the fuzzy controller that is profit for very complex PEMFC system [15]. Problems in this research, the rule bases are not produced in a systematic method, and the stability is not proved. Other problems are the selection of membership function type and optimization of fuzzy rules. The sliding mode control has been applied for fuel cell, such as the oxygen excess ratio control in [16] and power management in [17]. The popularity of sliding mode control method is because of its applicability to a class of nonlinear systems in the global sense, and the issues of performance and stability robustness to modeling uncertainties and disturbances. The major advantage of sliding mode is low sensitivity to plant parameter uncertainties and external/internal disturbances, which eliminates the necessity of exact modeling [18, 19]. Although unfortunately, the discontinuous control in sliding mode control causes the high-frequency switching. Therefore, high-frequency vibrations or "chattering" in the output damage actuators. One of the most beneficial techniques for chattering decreasing is higher order sliding mode control, which has been developed to decline this phenomenon and maintain robustness and finite time convergence properties of the classical sliding mode under load variations and parametric uncertainties.

Because of the most attractive features such as robustness against external disturbances and high accuracy and quick convergence in sliding mode algorithm, several sliding mode observer (SMO) for fault diagnosis approaches were developed for linear systems by Edwards et al. [16, 17]. However, conventional sliding mode technique induces undesirable chattering effect in control signals, which is due to the sign function. This phenomenon provides the system instability or actuator damaging. In recent years, the chattering effect was eliminated by High Order Sliding Mode (HOSM) technique because of its continuous output signal and guarantees the robustness against model uncertainties and internal or external disturbances.

Therefore, Liu et al. [20], super twisting (ST) sliding mode observer or fault diagnosis and isolation (FDI) schemes to estimate the system state and the fault signal in PEMFCs system was developed. In this estimator, the fault signal is successfully reconstructed based on the ST sliding mode algorithm without chattering phenomenon.

During the last years, nonlinear approaches based on fixed gain super twisting algorithm have been proposed for three-phase power converters by Liu et al. [21]. This controller system has a cascaded configuration which consists of two loops. The outer loop adjusts capacitor voltage of the DC-link, and the control law is based on super twisting algorithm. The inner control loop adjusts the actual currents to their desired that is designed using the STA. The STA has the most attractive characteristic as the finite time asymptotic convergence to requested value and chattering reduction.

Liu et al. [22] proposed a new control approach for the three-phase two-level AC/DC converters. The outer loop which adjusts DC-link capacitor voltage used a robust H∞ controller with an extended state observer. The inner loop strategy is applied to track the reactive/active power to desired values by second-order sliding mode (SOSM) technique. The comparison results with other controllers in this paper show that the developed strategy based on

SOSM controller has an exact tracking against load fluctuations.

High-order sliding mode for controlling the oxygen excess ratio (stoichiometry) in the literature [23, 24, 25] proposed to prevent irreversible damages in a polymer membrane due to the oxygen starvation phenomenon, in which the discontinuous control is applied on some higher time derivative of the system. The advantages of the proposed method are the robust stability, convergence to the sliding surface in finite time, and the reducing of chattering.

Kunusch et al. [7, 27] used a second-order sliding mode strategy by super twisting algorithm to stabilize the system and prevent chattering phenomenon in PEMFC. The STA controller provides a smoother signal control than what offers a sliding mode. Using a second-order sliding mode control, Laghrouche et al. [23, 24, 28, 29] suggested that may have resulted in the better transient response against fast variation of the current load. Control law based on the nonlinear optimization method to reduce chattering, stability in the tracking of the oxygen excess ratio, and optimization of the net power on PEMFC. He also proposed second-order sliding mode control in cascade configuration with a super twisting algorithm to improve output net power and maintaining of λ_{O_2} between 2 and 2.4 [6]. However, the STA and HOSM with fix gain are not able to compensate for the larger class of unknown perturbation in the severe nonlinearity of the fuel cell system.

Other options in [30] are made to control a knee exoskeleton as a wearable robot using a SOSM control. This control scheme helps the motions of the knee joint by the orthosis actuator. The SOSM strategy was developed to alleviate the chattering phenomenon consists of fast changing of the control signal that it can be dangerous for the actuators.

In [31] as a different type research, is proposed with second-order and conventional sliding mode algorithm for DC-DC buck converter. A comparison study between first-order sliding mode control and SOSM algorithm was developed. The advantages of the SOSM strategy are to suppress chattering and maintain robustness and finite time convergence comparison with conventional sliding mode control. However, in that research, fixed gain controller was considered when designing the controller. Furthermore, theoretical analysis of the system stability was not conducted.

Another application of variable gain STA strategy developed to wind energy conversion optimization is proposed by Evangelista et al. [32] and [33]. This control strategy compared with standard sliding mode strategy and concluded that mechanical stresses are reduced by this method to minimal level, and also the output chattering is reduced.

Gonzalez et al. [34] in 2012 implemented a variable gain control of a mass-spring system by providing a new technique for measuring the noise bounds. Gonzalez compared three typical such as fixed gain STA, variable gain STA, and traditional sliding mode and after implementation of these systems, they found out that the first-order sliding mode control had been chattering, and it was significantly decreased by both STA. Moreover, the result showed that compared to the classic STA, the variable gain STA could compensate for the larger class of perturbation and to reduce the chattering. Some research studies have been investigated the Lyanpunov stability theory and therefore, several approaches had been suggested to prove this theory and calculation of the finite time [35–38].

Moreno [36] proposed comprehensive of Lyapunov stability theory in super twisting algorithm that includes second-order sliding mode, and many other continuous algorithms, with constant or time-varying gains, and considering perturbations. Two distinct strict and robust Lyapunov functions are developed: a quadratic and a nonquadratic one. Each of them is useful to establish different properties of the algorithms. The quadratic Lyapunov functions are used to determine finite time convergence and to estimate the convergence time from every initial condition.

Motivation

In this research, we are interested in fast regulating the oxygen excess ratio and optimization of the net power output. To achieve this objective, a variable gain super twisting algorithm is used for air compressor control. Sliding mode control has already been made to fuel cell-related applications, such as stack breathing control in [39, 40] and second-order sliding mode control for stack breathing in [23, 24, 26]. The proposed control law developed to counteract the chattering phenomenon and to maintain robustness against the unknown bounds of uncertainties and perturbations in the PEMFC with severe nonlinearity and finite time convergence is obtained.

Contribution

The robust nonlinear adaptive gain super twisting sliding mode control is proposed for the control of an air feed system in PEMFC with a formalization of parametric uncertainties. So, the key-point of this paper is to consider the unknown bounds of uncertainties and perturbations in the PEMFC with severe nonlinearity. The accurate tracking and stability in a close-loop system of the oxygen excess ratio are proposed and a fast response time in order to avoid oxygen starvation during load variations is achieved. Furthermore, this paper provide:

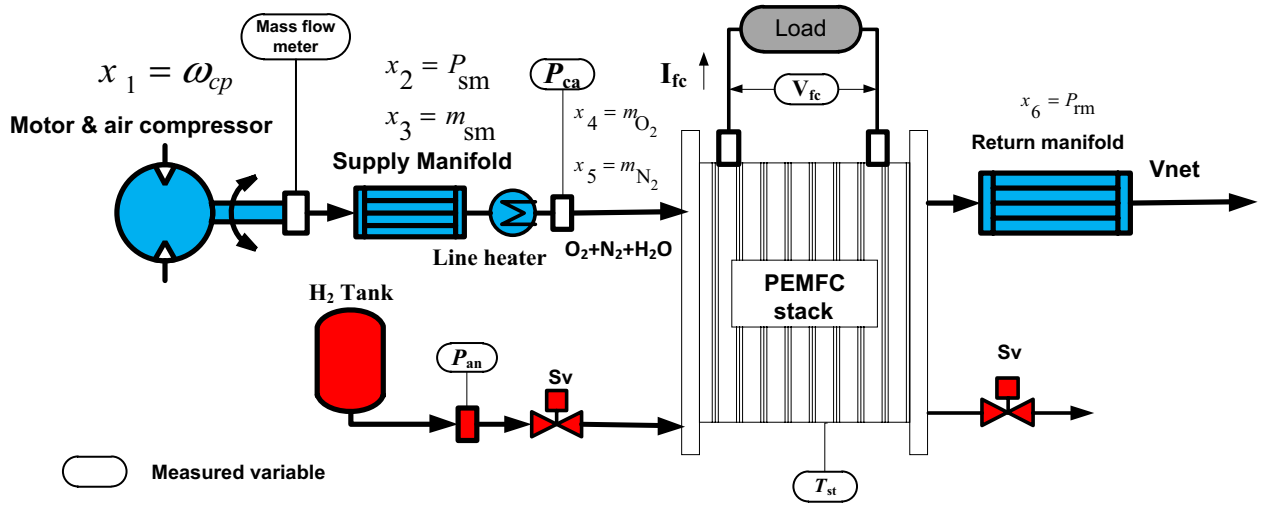

Figure 1. Block diagram of the fuel cell system with state representation.

1. The novel *adaptive* STA control law is designed for a PEMFC as a severe nonlinear system with special features such as the robustness, relative simplicity, and finite convergence time as a new strategy for PEMFC system.
2. The experimental noises and drift uncertainty terms/disturbances *with unknown boundary* for PEMFC nonlinear equations are rejected by the VGSTA.
3. A controller based on Lyapunov theory is designed to assure uniform stability of a nonlinear system considering bounding functions for disturbances and uncertainties of a realistic PEMFC model.
4. This proposed controller is explored and main advantages are summarized as follows:

   a. Robust regulation of the oxygen excess ratio to prolong the life span with chattering effect avoiding;
   b. Raising transient performance features with finite convergence time;
   c. More robustness to drift uncertain parameters and highly variation of load current with unknown boundary compared with the first-order SM and ST with fixed gains;
   d. Guaranteed extended range of operation, in spite of the severe nonlinearity of plant;
   e. Simple controller implementation, resulting in low computational costs in real-time environment.

The structures of this paper are organized into these sections: The dynamic model of the PEMFC air breathing system is discussed in Section 2. In Section 3, methodology and design of controller law according to Lyapunov's stability is discussed, and the results are presented in Section 4. Finally, the conclusion is presented in Section 5.

Fuel Cell System Dynamic Model

Dynamic models of the compressor, cathode humidifier, line heaters, and fuel cell stack channels were developed and validated. The model is suitable for nonlinear control design. Dynamic model has six states defined as: $X=[\omega_{cp},P_{sm},m_{sm},P_{O_2},P_{N_2},P_{rm}]^T$ where motor angular speed, ω_{cp}; supply manifold pressure, P_{sm}; mass of supply manifold, m_{sm}; oxygen pressure, P_{O_2}; nitrogen pressure, P_{N_2}; and return manifold pressure, P_{rm}. The air is mixed with these two gases such as the oxygen and nitrogen, nitrogen 79% and oxygen 21%, that is supplied to the cathode side. A schematic diagram of a PEM fuel cell stack together with some of its auxiliary is depicted in Figure 1.

The states are defined in following definitions:

States	Descriptions
$x_1 = \omega_{cp}$ (rad/sec)	Motor angular speed
$x_2 = P_{sm}$ (atm)	Supply manifold pressure
$x_3 = m_{sm}$ (kg)	Air mass in the supply manifold
$x_4 = P_{O_2}$ (atm)	Oxygen pressure in cathode side
$x_5 = P_{N_2}$ (atm)	Nitrogen pressure in cathode side
$x_6 = P_{rm}$ (atm)	Return manifold pressure

The state space model with six state are in equations (1–6). The complete set of equations is not included here for space reasons and can be found in [41]. They are:

$$\dot{x}_1 = \tau_{cm} - \tau_{cp} = \frac{\eta_{cm}}{J_{cp}}\frac{k_t}{R_{cm}}\left(v_{cm} - k_v x_1\right) - \frac{\tau_{cp}}{J_{cp}} \quad (1)$$

$$\dot{x}_2 = \frac{\gamma R_a}{V_{sm}}\left(-K_{sm,out}x_2 + +K_{sm,out}P_{v,ca} + K_{sm,out}\frac{x_5}{M_{N_2}} + K_{sm,out}\frac{x_4}{M_{O_2}}\right) \frac{\gamma x_2}{x_3} + W_{cp}\left(T_{atm} + \frac{T_{atm}}{\eta_{cp}}\left(\frac{x_2}{P_{atm}}\right)^{\frac{\gamma-1}{\gamma}} - 1\right) \quad (2)$$

$$\dot{x}_3 = W_{cp} - K_{sm,out}x_2 + K_{sm,out}P_{v,ca} + K_{sm,out}\frac{x_5}{M_{N_2}} + K_{sm,out}\frac{x_4}{M_{O_2}} \quad (3)$$

$$\dot{x}_4 = -\frac{x_4 K_{ca,out}}{m_{O_2}+m_{N_2}+\frac{P_{v,ca}V_{ca}M_v}{R_v T_{st}}}\left(-x_6 + P_{v,ca} + \frac{x_5}{M_{N_2}} + \frac{x_4}{M_{O_2}}\right) + y_{O_2,in}K_{sm,out}\frac{(R_{O_2}T_{st})}{V_{ca}} \times \left(x_2 - \frac{x_4}{M_{O_2}} - P_{v,ca} - \frac{x_5}{M_{N_2}}\right) - n\frac{(R_{O_2}T_{st})}{V_{ca}}\frac{M_{O_2}}{4F}I_{st} \quad (4)$$

$$\dot{x}_5 = \left(1 - X_{O_2}\right)(1+\Omega_{atm})^{-1}K_{sm,out}\frac{R_{N_2}T_{st}}{V_{ca}}\left(x_2 - \frac{x_4}{M_{O_2}} - \frac{x_5}{M_{N_2}} - P_{v,ca}\right) K_{sm,out}\frac{R_{N_2}T_{st}}{V_{ca}} \quad (5)$$

$$\dot{x}_6 = \frac{R_a T_{rm}}{V_{rm}}\left(K_{ca,out}\left(\frac{x_4}{M_{O_2}} + \frac{x_5}{M_{N_2}} + P_{v,ca} - x_6\right) - \left(P_{a_6}x_6^5 + P_{a_5}x_6^4 + P_{a_4}x_6^3 + P_{a_3}x_6^2 + P_{a_2}x_6 + P_{a_1}\right)\right) \quad (6)$$

In this model, the compressor motor voltage ($u = V_{cm}$ (V)) is the input control, and the fuel cell stack current ($d = I_{st}$ (A)) can be measured as disturbance. The model parameters are given in Appendix. The equations (1–6) can be written in a compact state space form which is as follows:

$$\dot{x} = f(x) + g(x).u + \phi(x).d \quad (7)$$

$$\dot{x} = \begin{bmatrix} f_1(x_1,x_2) \\ f_2(x_1,x_2,x_3,x_4,x_5) \\ f_3(x_2,x_4,x_5) \\ f_4(x_2,x_4,x_5,x_6) \\ f_5(x_2,x_4,x_5,x_6) \\ f_6(x_4,x_5,x_6) \end{bmatrix} + \begin{bmatrix} \eta_{cm}\frac{k_t}{J_{cp}R_{cm}} \\ 0 \\ 0 \\ 0 \\ 0 \\ 0 \end{bmatrix} \cdot u + \begin{bmatrix} 0 \\ 0 \\ 0 \\ -n\frac{M_{O_2}}{4F} \times \frac{R_{O_2}T_{st}}{V_{ca}} \\ 0 \\ 0 \end{bmatrix} \cdot d \quad (8)$$

where $x \in \mathbb{R}^6$ is the system state; $f \in \mathbb{R}^6 \to \mathbb{R}^6$ is a continuous vector function representing the dynamics of the autonomous system; $g \in \mathbb{R}^6$ and $\varphi(x) \in \mathbb{R}^6$ are vectors representing the input and the disturbance matrices, respectively. The compressor air flow (W_{cp}) is:

$$W_{cp} = B_{00} + B_{10}(P_{sm}) + B_{20}(P_{sm})^2 B_{01}(\omega_{cp}) + B_{11}P_{sm} + \omega_{cp} + B_{02}(\omega_{cp})^2 \quad (9)$$

Output voltage is expressed as a function of stack current, partial pressure, and temperature of fuel cell. The output stack voltage (V_{cell}) will be decreased due to ohmic losses, activation losses, and concentration losses. The output voltage is the difference between open circuit voltage and voltage losses, of which voltage losses are nonlinear functions of stack current, temperature, pressure, and chemical reactions. Thermodynamic potential, E, is defined using the Nernst equation in equation (11).

$$V_{cell} = E - \text{losses}, \quad \text{losses} = V_{activation} + V_{ohmic} + V_{concentration} \quad (10)$$

$$E = N\left(E_0 + \frac{RT}{2F}\left\{\frac{P_{H2}\left(\frac{P_{O_2}}{P_{OP}}\right)^{0.5}}{P_{H_2O_C}}\right\}\right) \quad (11)$$

$$V_{stack} = NV_{cell} \quad (12)$$

Also, the net power of the fuel cell system (P_{net}) is the difference between stack power and motor compressor power which is calculated by the following relationships:

$$P_{stack} = I_{st} \times V_{stack} \quad (13)$$

$$P_{auxiliary} = (V_{cm}) \times (V_{cm} - K_v \times x_1) \quad (14)$$

$$P_{net} = P_{Stack} - P_{auxiliary} \quad (15)$$

Oxygen excess ratio calculation

Reactants consuming in the fuel cell are faster than reactants supplied. For this reason, the starvation phenomenon occurs. Starvation happens especially during transient loads, and it is one of the main reasons of membrane damaging. Thus, fast regulation of the oxygen excess ratio by increasing the cathode mass flow is very significant. Furthermore, mass flow rising is limited by the actuator inertia. Therefore, the regulation of the oxygen excess ratio is a crucial issue [8, 42].

The oxygen excess ratio cannot be measured directly and has to be concluded from another sensing. Formula (16) shows clearly that it depends upon the ratio of two mass flows.

$$\lambda_{O_2} = \frac{\text{Oxygen Supplied}}{\text{Oxygen reacted}} = \frac{W_{O_2,in}}{W_{O_2,reacted}} \quad (16)$$

The oxygen flow reacting can be calculated by equation (16). It is proportional to the stack current. It can be written as:

$$W_{O_2,reacted} = M_{O_2}\frac{n.I_{st}}{4.F} \quad (17)$$

F = 96,485 C/mol is the Faraday constant, n the number of cells, and M_{O2} the molar mass of oxygen.

The calculation of the inlet oxygen flow ($W_{O2,in}$) is not straightforward. The inlet oxygen flow depends on the oxygen mass fraction ($X_{O2,in}$) and the inlet air flow ($W_{a,in}$):

$$W_{O_2,in} = X_{O_2,in} \cdot W_{a,in} \quad (18)$$

The inlet air flow ($W_{a,in}$) is equal:

$$W_{O_2,in} = X_{O_2,in} \cdot \frac{1}{(1+\Omega_{atm})} \cdot W_{sm,out} \quad (19)$$

The outlet flow in supply manifold is stated as a function of P_{sm} and cathode pressure (P_{ca}).

The outlet flow in the supply manifold ($W_{sm,out}$) is obtained from a linearized nozzle equation and then the following equations can be derived.

$$W_{sm,out} = K_{sm,out} \cdot (P_{sm} - P_{v,ca}). \tag{20}$$

Therefore, $W_{sm,out}$ is defined as follows:

$$W_{sm,out} = K_{sm,out} \cdot \left(x_2 - \frac{x_4}{M_{O_2}} \frac{R_{O_2} T_{st}}{V_{ca}} - \frac{x_5}{M_{N_2}} \frac{R_{N_2} T_{st}}{V_{ca}} - P_{v,ca} \right) \tag{21}$$

Thus, the inlet oxygen flow is derived by:

$$W_{O_2,in} = X_{O_2,in} \frac{1}{(1+\Omega_{atm})} \cdot K_{sm,out} \cdot \left(x_2 - \frac{x_4}{M_{O_2}} \frac{R_{O_2} T_{st}}{V_{ca}} - \frac{x_5}{M_{N_2}} \frac{R_{N_2} T_{st}}{V_{ca}} - P_{v,ca} \right) \tag{22}$$

Thus, λ_{O_2} is defined as the ratio between $W_{O2,in}$ and $W_{O2,reacted}$ in the fuel cell stack. Dependency of the stack current to the air flow $W_{O2,reacted}$ caused a severe drop in λ_{O_2}. In addition, the increasing of λ_{O_2}causes increasing of partial pressure of oxygen and then P_{Stack} will be improved. Therefore, the inlet air flow is identical with the compressor air flow. Regulation of the inlet air flow is equal to regulation of λ_{O_2} against the load fluctuations.

Methodology

In this section, the controller is developed according to a new version of the super twisting algorithm. There are some steps to do for controller designing:

1. The sliding variable should be defined to achieve the desired control objective.
2. The new set of variable should be described with changing of the variable S.
3. Next step is to determine the bounding functions g_2 and the first time derivative of g_2.
4. A Lyapunov function is selected to consider stability analysis and calculate controller adaptive gains.

Lyapunov function and controller design

In this work, a Lyapunov function is suggested for designing of variable gain super twisting algorithm in PEM fuel cell. A time invariant and nonsmooth, Lyapunov function is selected for appropriate perturbation-bound dependent gains for the STA. This controller can be directly used to the system with a relative degree (R.D) of 1. The adaptive gain's controller provides robust performance for regulation against severe uncertainty. There is a continuous and smooth control signal. Finite convergence time is guaranteed. The super twisting algorithm is a known algorithm in second-order sliding mode control that was introduced in [43, 44]. This algorithm can be written by equation (23) [43, 44], where $k_1(t)$ and $k_2(t)$ are gains and $\rho_1(t, x)$ and $\rho_2(t, x)$ are perturbation terms.

$$u_{VGSTA} = u_1 + u_2 \tag{23}$$

$$u_1 = -k_1(t)\phi_1(x_1) + u_2 + \rho_1(t,x)$$

$$\dot{u}_2 = -k_2(t)\phi_2(x_1) + \rho_2(t,x)$$

where the vector $\zeta^T = \Phi^T(x) = [\phi_1(s), u_2]$, $\phi_1(x_1) = k_c|S|^{\frac{1}{2}}\text{sign(s)}$, and $\phi_2(x_1) = \frac{k_c^2}{2}\text{sign(s)}$. The quadratic form of Lyapunov function can be written as follows [44]:

$$V_Q(x) = \zeta^T P \zeta \tag{24}$$

Matrix P, as a positive definite matrix, is symmetric and unique. Therefore, a Lyapunov function can be solved with an Algebraic Linear Equation (ALE) in the following equation:

$$A^T P + PA = -Q \tag{25}$$

where $A = \begin{bmatrix} -k_1 & 1 \\ -k_2 & 0 \end{bmatrix}$ and positive definite matrix $Q = Q^T > 0$. The $k_1(t)$ and $k_2(t)$ can be simplified to the following equations:

$$\phi_2(s) = \phi_1'(s)\phi_1(s) \tag{26}$$

$$\dot{\zeta} = \begin{bmatrix} \phi_1'(s)\{-k_1\phi_1(s) + s\} \\ -k_2\phi_2(s) \end{bmatrix} = \phi_1'(s) \begin{bmatrix} -k_1, 1 \\ -k_2, 0 \end{bmatrix} \zeta = \phi_1'(s) A \zeta \tag{27}$$

$$\dot{V}_Q(x) = \dot{\zeta}^T P \zeta + \zeta^T P \dot{\zeta} = \phi_1'(s)\zeta^T(A^T P + PA)\zeta = -\phi_1'(s)\zeta^T Q \zeta. \tag{28}$$

According to [34–36], variable gains are bounded to the following assumption:

$$|\boldsymbol{\rho}_1(\mathbf{t},\mathbf{x})| \le \mathbf{g}_1(\mathbf{t},\mathbf{x})|\boldsymbol{\phi}_1(\mathbf{x}_1)| \le \mathbf{k}_c|s|^{\frac{1}{2}}\mathbf{g}_1(\mathbf{t},\mathbf{x}) \tag{29}$$

$$\left| \frac{\mathbf{d}}{\mathbf{dt}} \boldsymbol{\rho}_2(\mathbf{t},\mathbf{x}) \right| \le \mathbf{g}_2(\mathbf{t},\mathbf{x}) \left| \boldsymbol{\phi}_2(\mathbf{x}_1) \right| \le \frac{\boldsymbol{k}_c^2}{2} \mathbf{g}_2(\mathbf{t},\mathbf{x}) \tag{30}$$

$$\begin{aligned} \boldsymbol{\rho}_1(\mathbf{t},\mathbf{x}) &= \boldsymbol{\alpha}_1(\mathbf{t},\mathbf{x})\boldsymbol{\phi}_1(\mathbf{s}), \left|\boldsymbol{\alpha}_1(\mathbf{t},\mathbf{x})\right| \le \left|\mathbf{g}_1(\mathbf{t},\mathbf{x})\right| \\ \boldsymbol{\rho}_2(\mathbf{t},\mathbf{x}) &= \boldsymbol{\alpha}_2(\mathbf{t},\mathbf{x})\boldsymbol{\phi}_2(\mathbf{s}), \left|\boldsymbol{\alpha}_2(\mathbf{t},\mathbf{x})\right| \le \left|\mathbf{g}_2(\mathbf{t},\mathbf{x})\right| \end{aligned} \tag{31}$$

$k_1(t)$, $k_2(t)$, and $K_c > 0$ are variable gains [45]. P matrix is considered as follows:

$$P = \begin{bmatrix} p_1 & p_3 \\ p_3 & p_2 \end{bmatrix} = \begin{bmatrix} \beta + 4\varepsilon^2 & -2\varepsilon \\ -2\varepsilon & 1 \end{bmatrix} \tag{32}$$

Stability conditions can be obtained with the desired positive definite matrix (Q) that is determined as follows:

$$Q-2\varepsilon I=\begin{bmatrix} 2\beta k_1+4\varepsilon(2\varepsilon k_1-k_2)-2(\beta+4\varepsilon^2)\alpha_1+4\varepsilon\alpha_2-2\varepsilon & * \\ k_2-2\varepsilon k_1-(\beta+4\varepsilon^2)+2\varepsilon\alpha_1 & 2\varepsilon \end{bmatrix} = \begin{bmatrix} 2\beta k_1-(\beta+4\varepsilon^2)(4\varepsilon+2\alpha_1)+4\varepsilon\alpha_2-2\varepsilon & * \\ 2\varepsilon\alpha_1-\alpha_2 & 2\varepsilon \end{bmatrix} \tag{33}$$

Q would be a positive definite matrix, if:

$$k_1>\frac{2\varepsilon\alpha_2+(\beta+4\varepsilon^2)(2\varepsilon+\alpha_1)+\varepsilon}{\beta} \tag{34}$$

$$k_2=2\varepsilon k_1+\beta+4\varepsilon^2 \tag{35}$$

Therefore, after the change of variables, the S variable is defined as a new variable. So, control law design is based on variable sets of $[Sx']$ and $x'\in\mathcal{R}^{n-1}$ is replaced with $x\in\mathcal{R}^n$. It can be easily separate from the part that is zeroed when $S = 0$ from the rest.

$$\dot{s}=f_s(t,x',s)+u_{\text{VGSTA}}=\underbrace{f_s(t,x',0)}_{\rho_2(t,x')}+\underbrace{[f_s(t,x',s)-f_s(t,x',0)]}_{\rho_1(t,x',s)}+u_{\text{VGSTA}} \tag{36}$$

Proposed controller gains in equation (23) can be calculated using the Lyapunov function for equation (37) as follows:

$$\begin{aligned} k_1(t,x',s)&=\delta+\tfrac{1}{\beta}\left\{\tfrac{1}{4\varepsilon}[2\varepsilon g_1+g_2]^2+2\varepsilon g_2+\varepsilon+[2\varepsilon+g_1(t,x)](\beta+4\varepsilon^2)\right\} \\ k_2(t,x',s)&=\beta+4\varepsilon^2+2\varepsilon k_1(t,x',s) \end{aligned} \tag{37}$$

where $\beta > 0$, $\varepsilon > 0$, and $\delta > 0$ are arbitrary positive constants and $g_1(t, x)$ and $g_2(t, x)$ are positive and in the process boundaries $\dot{\rho}_2(t,x),\rho_1(t,x)$ should be calculated.

Bounds on the perturbations

The design procedure needs finding of the bounding functions is made in the equations of $\rho_1(x', S, t)$ and the first derivative of $\rho_2(x', t)$ considering real values for their parameters, that is, changing from nominal values, and consisting of internal and external disturbances. The sliding surface is defined in equation (38). With change of the variable, the S variable becomes a member of the new set of variables in following:

$$S=W_{\text{cp}}-W_{\text{cp,ref}} \tag{38}$$

As a result:

$$S=B_{00}+B_{10}(x_2)+B_{20}x_2^2+B_{10}x_1+B_{11}x_2x_1+B_{02}x_1^2-W_{\text{cp,ref}} \tag{39}$$

Thus, the new value x_1 can be calculated as follows:

$$-S+B_{00}+B_{10}(x_2)+B_{20}x_2^2+B_{10}x_1+B_{11}x_2x_1+B_{02}x_1^2-W_{\text{cp,ref}}=0 \tag{40}$$

As result:

$$\begin{aligned} x_1=h(t,x',s)=&\left(\tfrac{-B_{11}}{2B_{02}}\right)x_2-\left(\tfrac{B_{10}}{2B_{02}}\right) \\ &\mp\sqrt{\left(\tfrac{{B_{11}}^2}{4{B_{02}}^2}-\tfrac{B_{20}}{2B_{01}}\right){x_2}^2+\left(\tfrac{2B_{02}B_{11}}{4{B_{02}}^2}-\tfrac{B_{10}}{B_{02}}\right)x_2+\left(\tfrac{{B_{10}}^2}{4{B_{02}}^2}-\tfrac{B_{00}}{2B_{02}}\right)+\tfrac{S+W_{\text{cp,ref}}}{B_{02}}} \end{aligned} \tag{41}$$

A new set of conditions for $x' = \{x_2, x_3, x_4, x_5, x_6\}$ defined. Consider the first-order derivative S:

$$\begin{aligned} \dot{S}&=\dot{W}_{\text{cp}}-\dot{W}_{\text{cp,ref}} \\ \dot{W}_{\text{cp}}&=[B_{10}+B_{11}x_{02}+2B_{02}h]\dot{x}_1+[B_{10}+2B_{20}x_2+B_{11}h]\dot{x}_2 \end{aligned} \tag{42}$$

Considering $D = [B_{10} + B_{11}x_2 + 2B_{02}h(t, x', s)]$ and with a replacement value $\dot{x}_1$ in following:

$$\begin{aligned} \dot{W}_{\text{cp}}=&DB_1K_1V_{\text{cm}}+D\left(-\left[\tfrac{c_p\times T_{\text{atm}}}{n_{\text{cp}}\times J_{\text{cp}}\times h}W_{\text{cp}}\left(\left(\tfrac{x_2}{P_{\text{atm}}}\right)^{B_4}-1\right)\right]+(-B_2hk_t)\right) \\ &+[B_{10}+2B_{20}x_2+B_{11}h]\dot{x}_2 \end{aligned} \tag{43}$$

As a result:

$$\begin{aligned} \dot{S}&=f_s(t,x',s)+g_s(x',s)v_{\text{cm}} \\ g_s(x',s)v_{\text{cm}}&=u_{\text{VGSTA}} \\ \dot{S}&=f_s(t,x',0)+[f_s(t,x',s)-f_s(t,x',0)]+u_{\text{VGSTA}} \end{aligned} \tag{44}$$

$$\begin{aligned} g_s(x',s)&=\tfrac{\partial s}{\partial v_{\text{cm}}}=D\times B_1K_1 \\ f_s(t,x',s)&=\tfrac{\partial s}{\partial x_2}\dot{x}_2+\tfrac{\partial s}{\partial x_1}\dot{x}_1 \\ f_s(t,x',s)&=D\left(-\left[\tfrac{c_p\times T_{\text{atm}}}{n_{\text{cp}}\times J_{\text{cp}}\times h}W_{\text{cp}}\left(\left(\tfrac{x_2}{P_{\text{atm}}}\right)^{B_4}-1\right)\right]+(-B_2hk_t)\right)+[B_{10}+2B_{20}x_2+B_{11}h]\dot{x}_2-\dot{W}_{\text{cp,ref}} \end{aligned} \tag{45}$$

The functions $\rho_1(x', S, t)$ and $\rho_2(x', t)$ are extracted:

$$\begin{aligned} \rho_2(x',t)&=f_s(t,x',0) \\ \rho_1(x',S,t)&=f_s(t,x',S)-f_s(t,x',0) \end{aligned} \tag{46}$$

$$\rho_2(x',t)=D(t,x',0)\left(-\left[\frac{c_p\times T_{\text{atm}}}{n_{\text{cp}}\times J_{\text{cp}}\times h}W_{\text{cp}}\left(\left(\frac{x_2}{P_{\text{atm}}}\right)^{B_4}-1\right)\right]+(-B_2h(t,x',0)k_t)\right)+[B_{10}+2B_{20}x_2+B_{11}h(t,x',0)]\dot{x}_2-\dot{W}_{\text{cp,ref}} \tag{47}$$

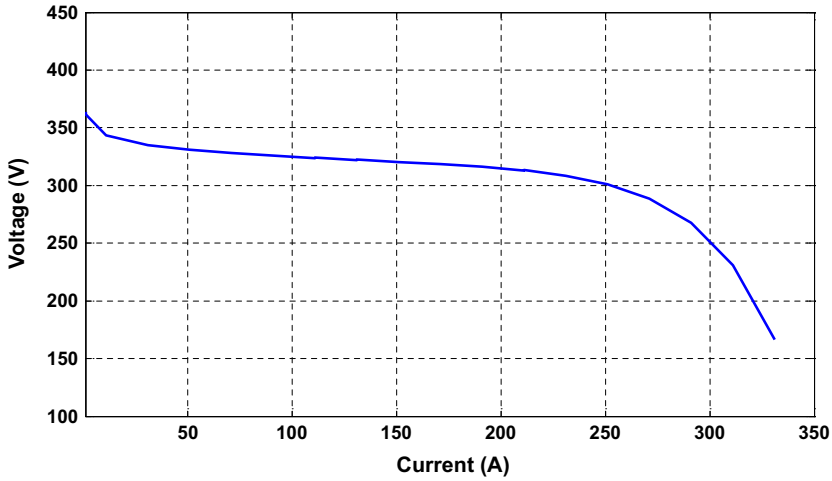

Figure 2. Polarization curve of proton exchange membrane fuel cell for $T = 50°C$.

$$\rho_1(x',S,t)=D(t,x',s)\left(-\left[\frac{c_p\times T_{\text{atm}}}{n_{\text{cp}}\times J_{\text{cp}}\times h}W_{\text{cp}}\left(\left(\frac{x_2}{P_{\text{atm}}}\right)^{B_4}-1\right)\right]+(-B_2h(t,x',s)k_t)\right)+[B_{10}+2B_{20}x_2+B_{11}h(t,x',s)]\dot{x}_2-\dot{W}_{\text{cp,ref}}-\rho_2(x',t) \quad (48)$$

As a result, $\rho_1(x', S, t)$ and $\rho_2(x', t)$ of the extension of equation (46) are obtained and $g_1(t, x)$ and $g_2(t, x)$ can be calculated. Due to the complexity of the equations, the calculation was performed by final values of $g_2(t, x)$ and $g_1(t, x)$ that were obtained from equation (31). According to equation (37), the variable gains finally were obtained.

Results and Discussions

The aim of this section is testing and verifying the performances of the designed VGSTA and the fixed gain super twisting algorithm in the PEMFC system with unknown bounded uncertainty in the MATLAB/Simulink environment.

Fuel cell model validation TEST

The PEMFC dynamic model in this paper is based on Ref. [41]. The model was simulated by equations (1–8). The net output power, the oxygen excess ratio, and compressor flow rate (eqs. 9, 15 and 16) were calculated. The model is based on simulating the relationship between the output voltage and states of an air feed system. Figures 2 and 3 show a polarization curve that is the output voltage against load current and output power versus load current at steady state for operating temperature 50°C. Using equations (1–15) of the state space and voltage and power equations of PEMFC, the polarization (V-I) and power (P-I) curves of the system indicated in Figures 2–4 were established for 80 kW. This stack is composed of $N_{\text{cell}} = 381$.

The V-I and P-I curves are shown in Figure 4A and B. It is shown that the normal operation behavior of a fuel cell with temperature increasing from 30°C to 80°C causes the power to increase gradually to the maximum power point and then decrease. In order to consider the efficiency of the suggested new controller, simulation was made in the MATLAB/Simulink environment. The block diagram of the close-loop system is shown in Figure 5.

In Figure 6 is shown a block diagram of the control system. The sliding surface was calculated by the W_{cp} and $W_{\text{cp,ref}}$. Finally, $k_1(t)$ and $k_2(t)$ gains, and the control input of VGSTA were obtained. In fact, variation current loads are applied at t = 20s, 55s, 80s, and 130s. Figure 7 shows stack current that is applied as a disturbance to the system. Figure 8 shows states for the close-loop system based on variable gains super twisting controller. It is observed from the figure that the state x_1 or the angular velocity has an acceptable range, which is changed between 6261 and 25046 g. The air mass in supply manifold was changed between 0.03 and 0.05 kg with the load current variations. The pressure values of the states x_2, x_4, x_5, and x_6 are in the bounded suitable pressure ranges which show that the system states have appropriate condition.

The oxygen excess ratio in the proposed controller is compared with fixed gain controller in Figure 9A. It is shown that both controllers are capable of reducing the chattering phenomenon. Furthermore, it is obviously

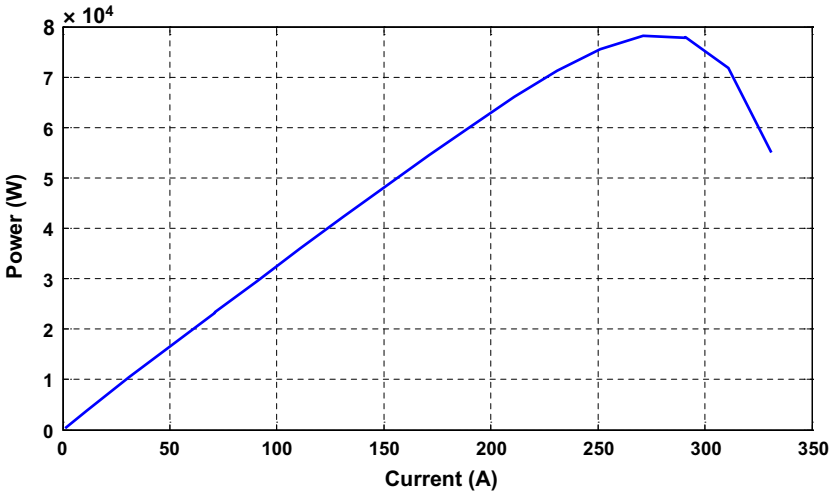

Figure 3. P-I curve of proton exchange membrane fuel cell for $T = 0°C$.

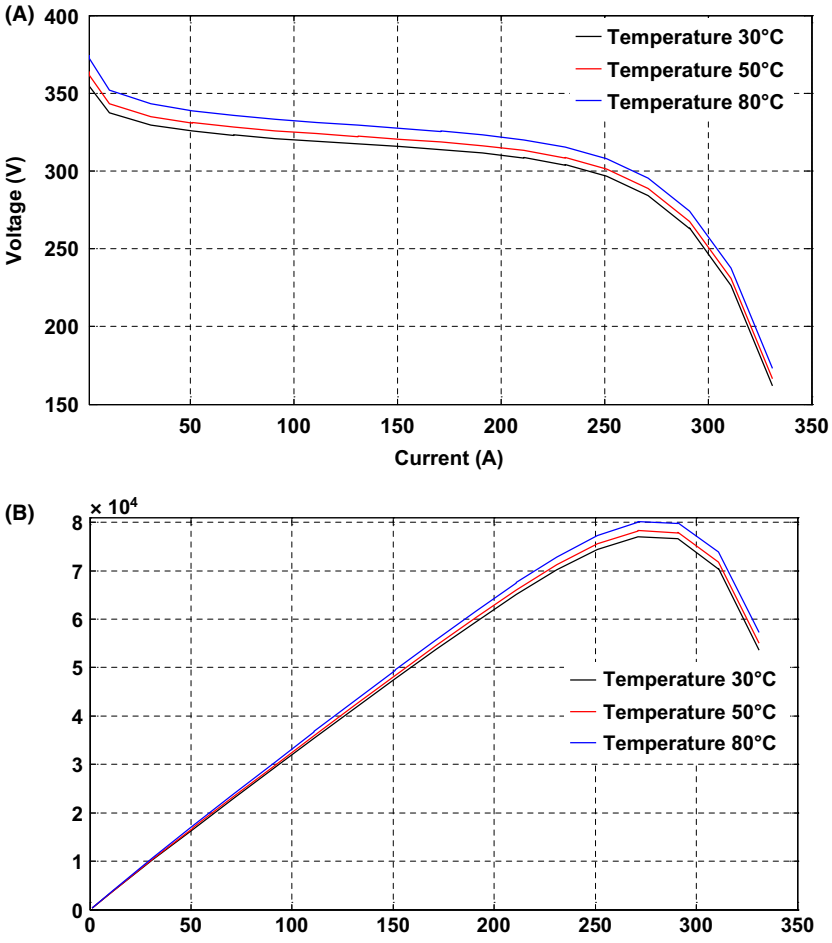

Figure 4. (A) Polarization curve. (B) P-I curve of proton exchange membrane fuel cell for different temperatures.

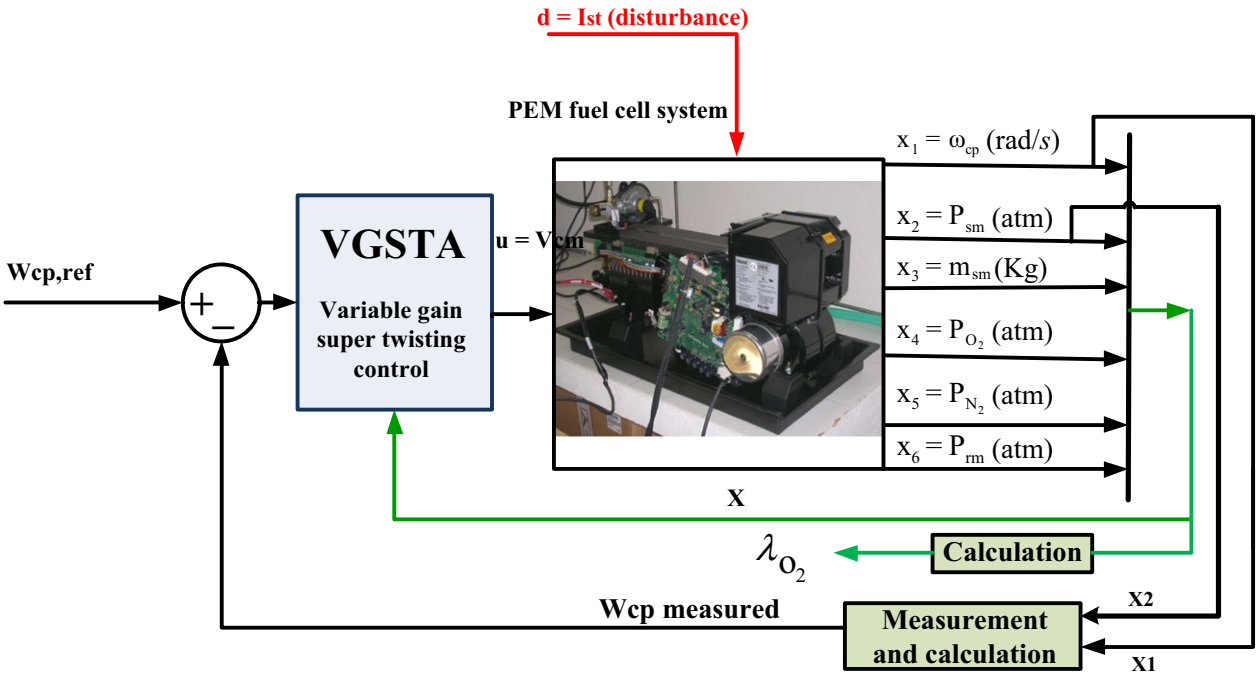

Figure 5. Block diagram of the close-loop system based on variable gain super twisting algorithm.

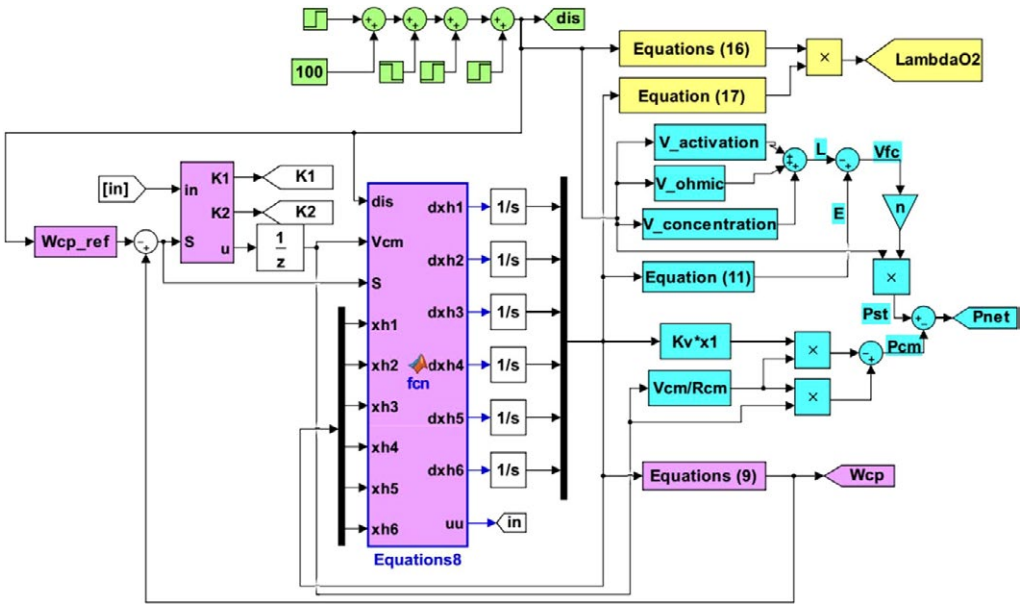

Figure 6. Block diagram of the close-loop system in MATLAB/Simulink.

indicated that using the VGSTA, the λ_{O_2} of PEMFC is achieved quickly with great precision and global stability of the close-loop system to the desired value of 2. However, the fixed gain controller could not track the set-point value. There is a difference in the value of λ_{O_2} for all ranges of load current, and it does not follow a desired constant value. It has a deviation from the desired values about 0.5–0.8.

Figure 9B shows a comparison between the net output powers in the proposed controller and the fixed gain STA. It was concluded from this figure that the net output power increased in the applied variable gain condition,

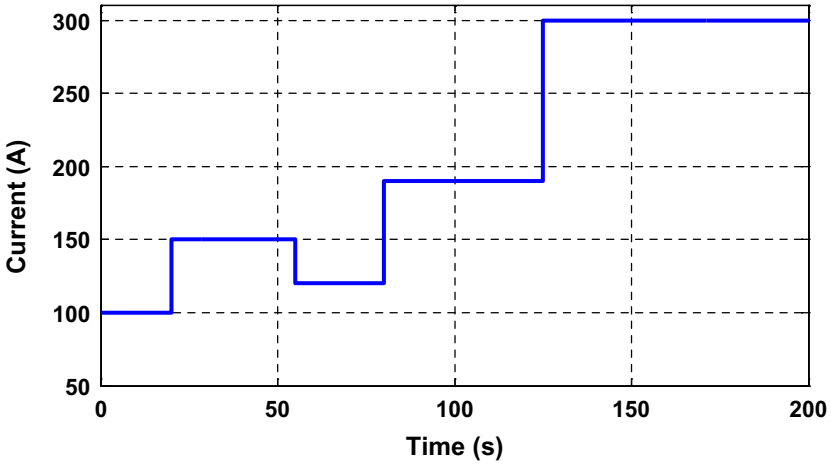

Figure 7. The load current variation as disturbance.

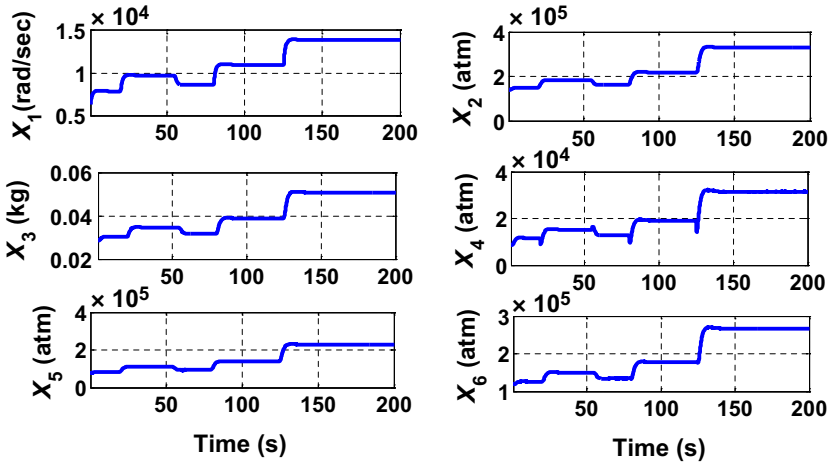

Figure 8. States profile in the case of the variable gain controller.

and the fuel cell generated an output net power of about 25–50 kW for VGSTA proposed method, but it is 25–40 kW in fixed gain STA, the highest current (it is shown at t = 55 sec). Therefore, there is a suitable saving in the output net power. There is 'start up' peak that is shown on the figures because of unexpected step load current. Because of a sudden changing of load current at t = 20, 55, 80, and 130 sec, results have a 'start up' peak at these times in oxygen excess ratio and net output power.

The variable gains $k_1(t)$ and $k_2(t)$ are shown in Figure 10, and it was clear from the figure that the gains $k_1(t)$ and $k_2(t)$ had a value about 5 and 1.5, respectively.

Parameters variations as unknown uncertainty

In order to validate the robustness of the proposed controller, some PEMFC parameters were changed under permissible bound of variation as the uncertainty in Table 1 [41].

In real condition, the actual and nominal value of the parameters into the PEMFC system cannot be accurately achieved. They are sensitive to the ambient circumstances (e.g., temperature, pressure, etc.) and structural characteristics (e.g., manifold volumes, rotor inertia, motor resistance, motor inductance, etc.). The main issue of the PEMFC model is the existence of unknown parametric uncertainties and variations that motivate using of new control strategy. Although, the PEMFC system is a severe non-linear model and the proposed novel VGSTA is suitable for this system. The Figure 11A shows that the net power against the load current variation in the presence or absence of uncertainty is almost identical variation in both of them.

Figure 11B shows the behavior of the oxygen excess ratio under load variations and parametric uncertainties, compared to behavior of the nominal system under the same controller gains. It can be seen that the controller

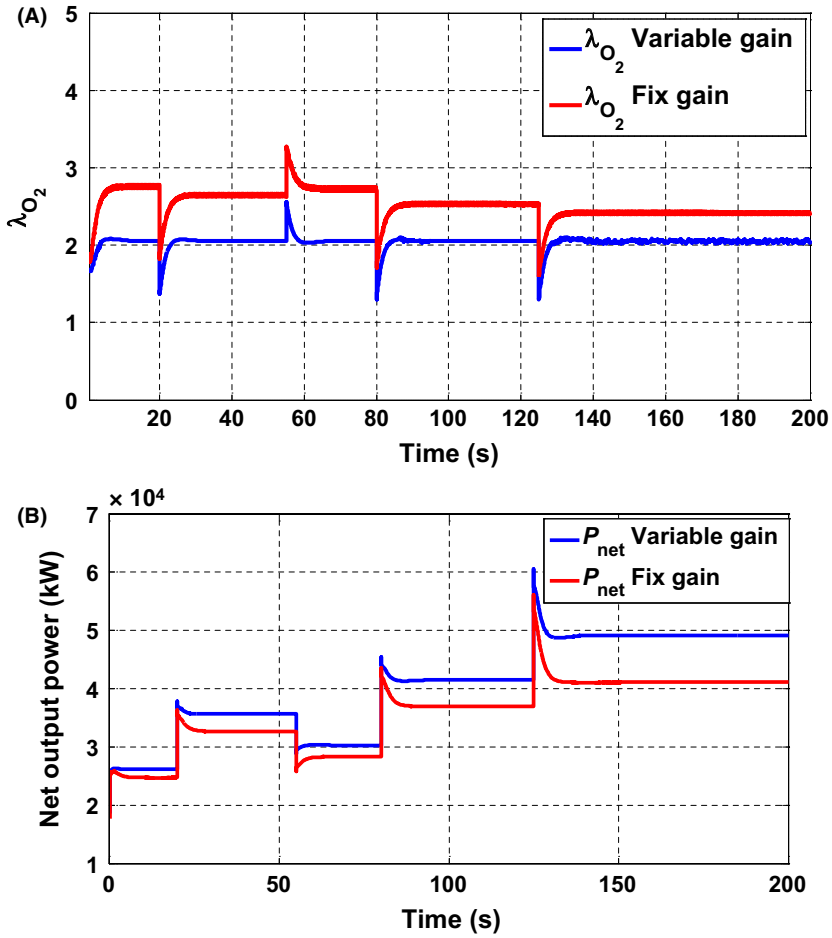

Figure 9. (A) Oxygen excess ratio in the case of variable and fix gain controller. (B) Net output power in the case of variable and fixed gain controller.

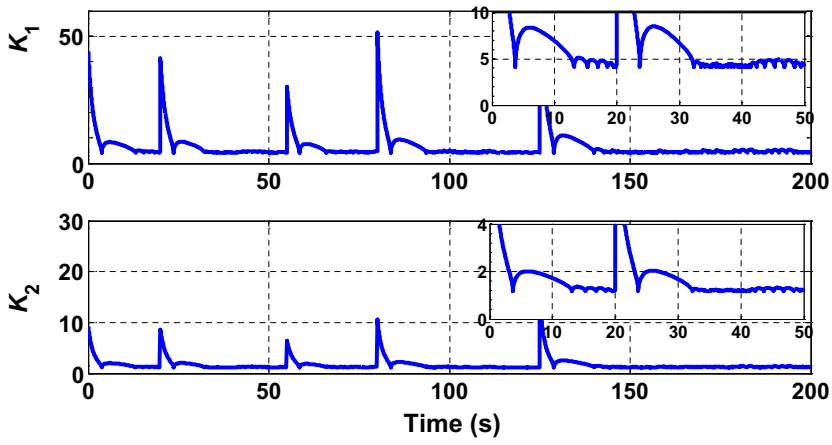

Figure 10. Variable gains.

has robustness against the uncertainty in the system and the λ_{O_2} tracks the desired value 2. Variable gains in the perturbed condition are shown in Figure 12.

Realistic measurement noise test

A noise test has been applied in addition to the parameter uncertainty. Considering that the common values of signal/

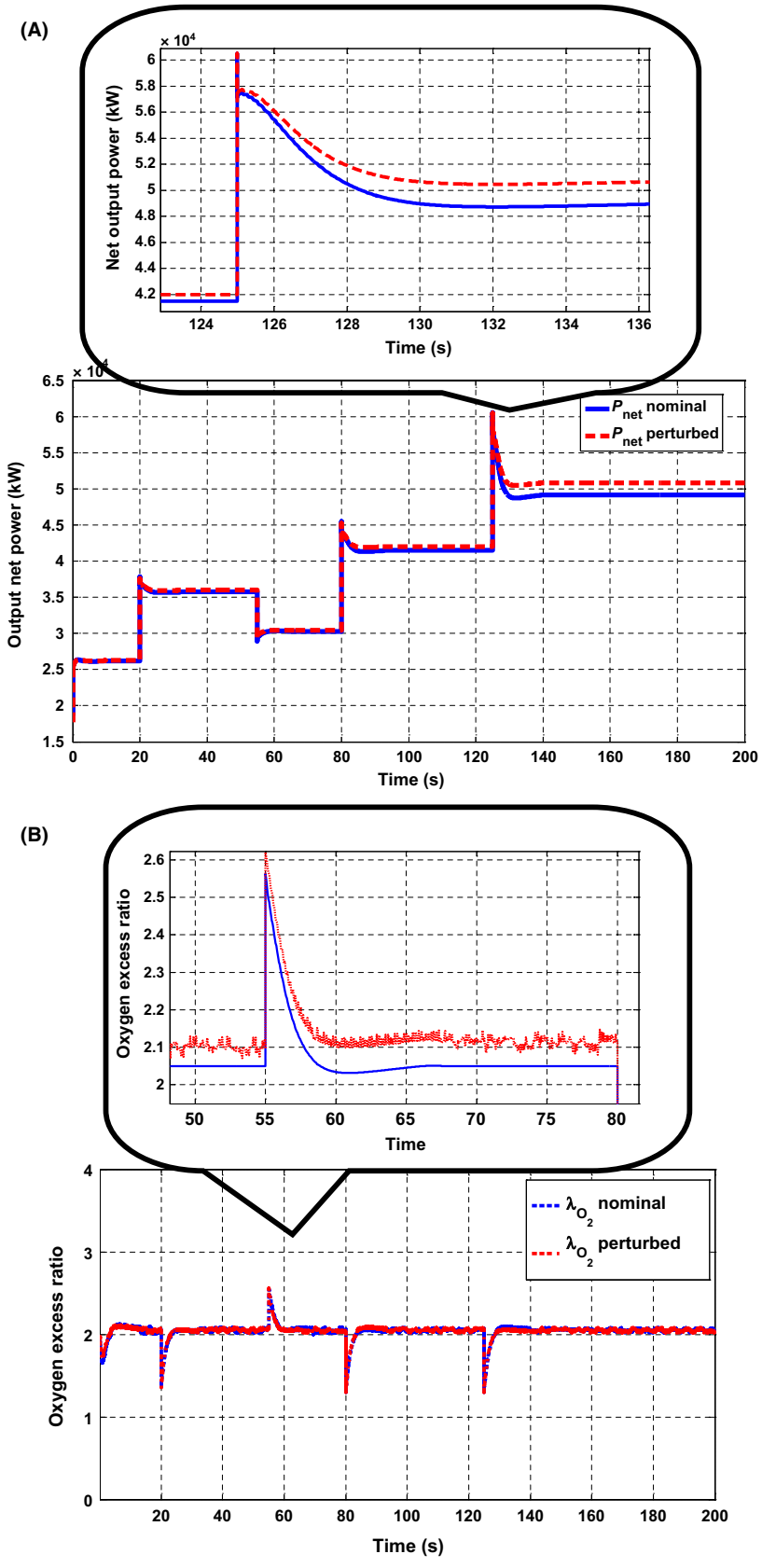

Figure 11. (A) Output net power in the perturbed condition. (B) Oxygen excess ratio in the perturbed condition.

noise (SNR) are about 28 [dB], all measurements were with power transmission equal to PSD = 0.22 [W], and then a distribution noise is Gaussian with mean value = 0.0023237, variance = 0.13362, and covariance = 0.0179 [41].

Figure 13 shows states profile in the case of the variable gain controller under realistic noise condition. Figure 14 indicates the noise and noise-free profiles of the measured quantities. It shows the appearance of small variation of the λ_{O_2}. It confirms the proposed controller regulates accurately also in the simultaneous presence of noise and parameter uncertainties.

Table 1. Bound of parameter variations [41].

Parameters	Uncertainty
Temperature of the stack (T_{st})	+10%
Single stack cathode volume (V_{ca})	+5%
Motor constant (k_v)	−10%
Electrical resistance of motor (R_{cm})	+5%
Diameter Compressor (d_c)	+1%
Motor inertia (J_{cp})	+10%
Atmospheric pressure (P_{atm})	+10%
Supply manifold volume (V_{sm})	−10%
Return manifold volume (V_{rm})	−10%

Conclusion

In this paper, a variable gain super twisting controller as a second-order sliding mode for the air breathing system of the PEM fuel cell is proposed. The PEMFC model is on sixth order and severe nonlinear model. The proposed controller is designed via Lyapunov theory and by using simulation, taking into account uncertainty, and experimental noises are validated and provided acceptable results. The suitability, accuracy, and high performance of the suggested controller through comparison with fixed gain was shown. This design method needs the calculation of bound of disturbance for controller design, and this method reduces online calculations against another nonlinear and robust controller such as H∞ and adaptive control law that are very complex. Structure of the algorithm is simple,

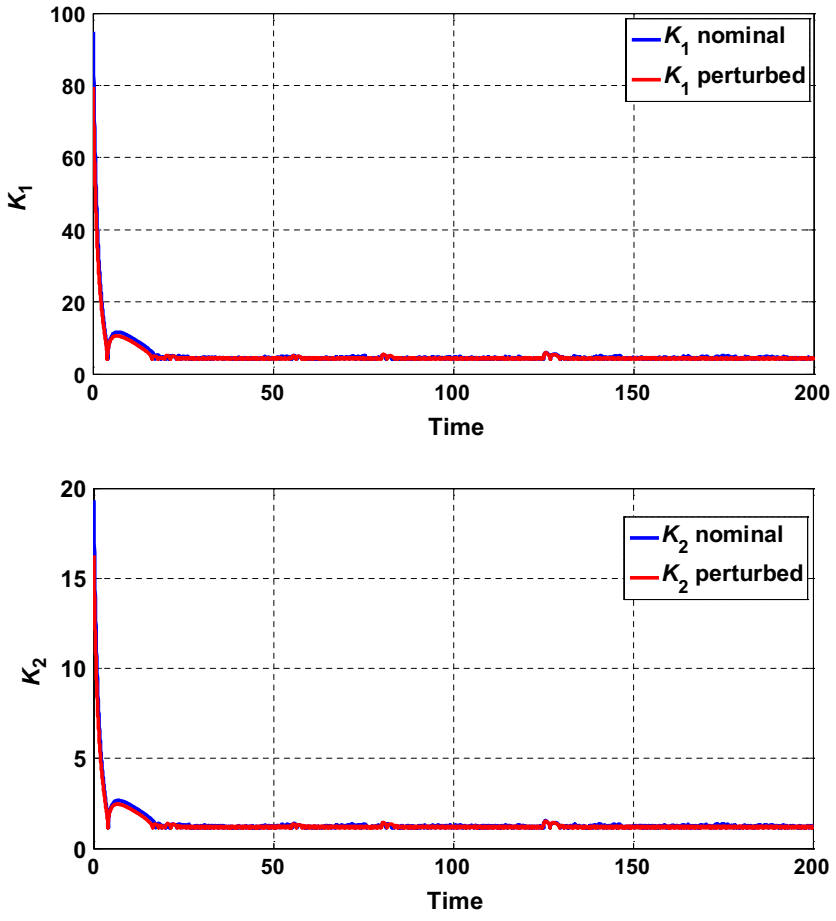

Figure 12. Variable gains in the perturbed condition.

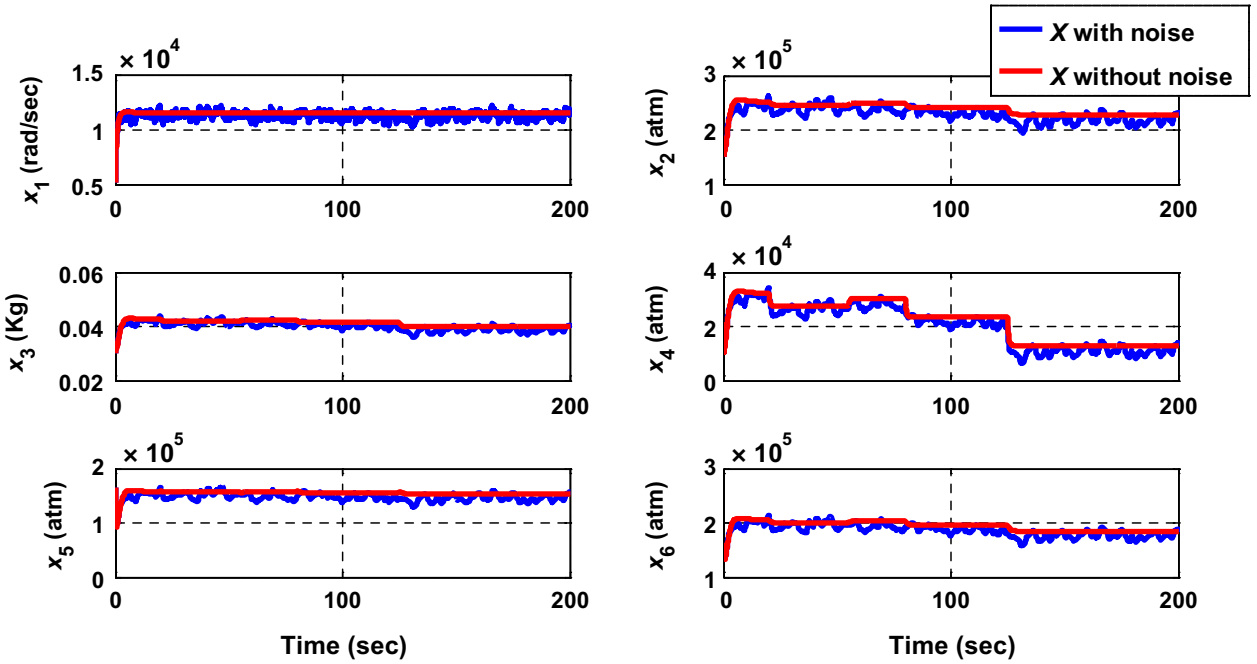

Figure 13. States profile in the case of the variable gain controller under realistic noise condition.

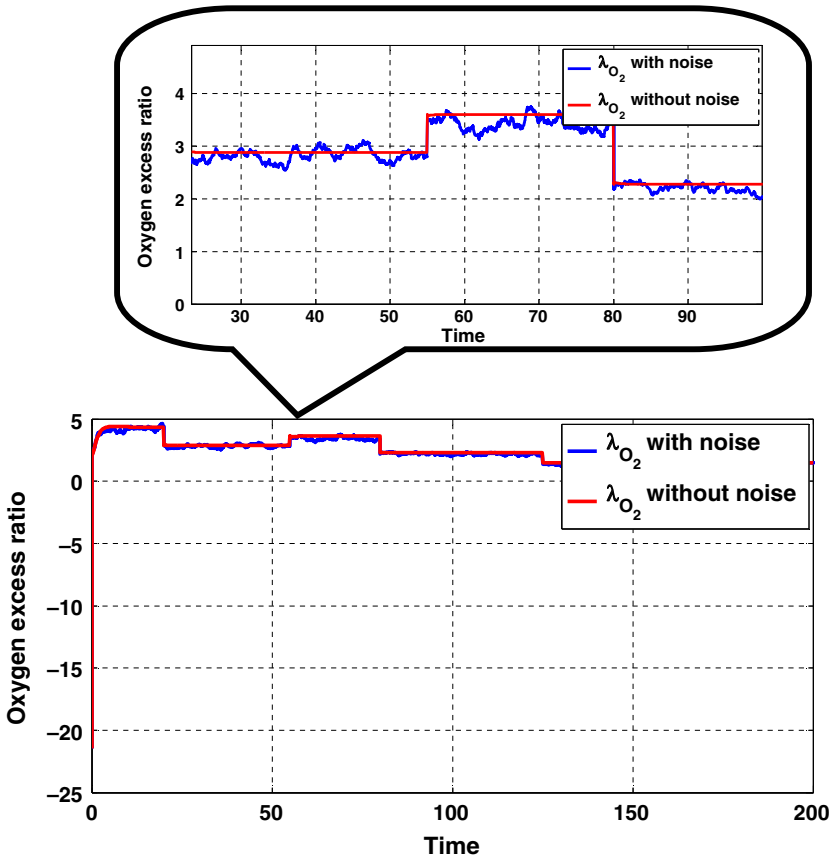

Figure 14. Oxygen excess ratio under practical noise condition.

thus low online computation is required. The variable gain controller is very precise in set-point tracking of the oxygen excess ratio and improves the net output power compared with fixed gain controller. In result section, extra uncertainty has been incorporated in several parameters of the system (Table 1) and the robustness against the realistic measurement noise, and uncertainty was considered and verified. Reduction of chattering, simplicities of implementation, and finite time convergence are the advantages of the proposed controller. A formal proof of stability based on the Lyapunov function and also calculation of the adaptive gains is presented. The simulation results show that regulation of the λ_{O_2} is more robust than fixed gain super twisting algorithm with the better transient response under parametric uncertainties, load variations, and noisy circumstances to avoid oxygen starvation during load variations.

Conflict of Interest

None declared.

References

1. Herrmann, T., M. Dillig, M. Hauth, and J. Karl. 2017. Conversion of tars on solid oxide fuel cell anodes and its impact on voltages and current densities. Energy Sci. Eng. 5:194–207.
2. Meidanshahi, V., and G. Karimi. 2012. Dynamic modeling, optimization and control of power density in a PEM fuel cell. Appl. Energy 93:98–105.
3. Bizon, N. 2011. Nonlinear control of fuel cell hybrid power sources: part I–Voltage control. Appl. Energy 88:2559–2573.
4. Zhang, X., M. Ni, W. He, and F. Dong. 2015. Theoretical analysis and optimum integration strategy of the PEM fuel cell and internal combustion engine hybrid system for vehicle applications. Int. J. Energy Res. 39:1664–1672.
5. Matraji, I., S. Laghrouche, S. Jemei, and M. Wack. 2013. Robust control of the PEM fuel cell air-feed system via sub-optimal second order sliding mode. Appl. Energy 104:945–957.
6. Matraji, I., S. Laghrouche, and M. Wack. 2011. Cascade control of the moto-compressor of a PEM fuel cell via second order sliding mode. 50th IEEE Conference on Decision and Control and European Control Conference (CDC-ECC).
7. Kunusch, C., P. F. Puleston, M. A. Mayosky, and L. Fridman. 2013. Experimental results applying second order sliding mode control to a PEM fuel cell based system. Control Eng. Pract. 21:719–726.
8. Pukrushpan, J. T., A. G. Stefanopoulou, and H. Peng. 2004. Control of fuel cell power systems: principles, modeling, analysis and feedback design. Springer Science & Business Media, London.
9. Tang, Y., W. Yuan, M. Pan, Z. Li, G. Chen, and Y. Li. 2010. Experimental investigation of dynamic performance and transient responses of a kW-class PEM fuel cell stack under various load changes. Appl. Energy 87:1410–1417.
10. Liu, J., Y. Gao, X. Su, M. Wack, and L. Wu. 2018. Disturbance-observer-based control for air management of PEM fuel cell systems via sliding mode technique. IEEE Trans. Control Syst. Technol. 99:1–10. https://doi.org/10.1109/TCST.2018.2802467
11. Wu, L., Y. Gao, J. Liu, and H. Li. 2017. Event-triggered sliding mode control of stochastic systems via output feedback. Automatica 82:79–92.
12. Niknezhadi, A., M. Allué-Fantova, C. Kunusch, and C. Ocampo-Martínez. 2011. Design and implementation of LQR/LQG strategies for oxygen stoichiometry control in PEM fuel cells based systems. J. Power Sources 196:4277–4282.
13. Na, W. K., and B. Gou. 2008. Feedback-linearization-based nonlinear control for PEM fuel cells. IEEE Trans. Energy Convers. 23:179–190.
14. Li, Q., W. Chen, Y. Wang, J. Jia, and M. Han. 2009. Nonlinear robust control of proton exchange membrane fuel cell by state feedback exact linearization. J. Power Sources 194:338–348.
15. Benchouia, N. E., A. Derghal, B. Mahmah, B. Madi, L. Khochemane, and E. Hadjadj Aoul. 2015. An adaptive fuzzy logic controller (AFLC) for PEMFC fuel cell. Int. J. Hydrogen Energy 40:13806–13819.
16. Tan, C. P., and C. Edwards. 2003. Sliding mode observers for robust detection and reconstruction of actuator and sensor faults. Int. J. Robust Nonlinear Control 13:443–463.
17. Yan, X.-G., and C. Edwards. 2008. Adaptive sliding-mode-observer-based fault reconstruction for nonlinear systems with parametric uncertainties. IEEE Trans. Industr. Electron. 55:4029–4036.
18. Levant, A. 2007. Principles of 2-sliding mode design. Automatica 43:576–586.
19. Utkin, V. I. 2008. Sliding mode control: mathematical tools, design and applications. Pp. 289–347 *in* A. A. Agrachev, A. Stephen Morse, E. D. Sontag, H. J. Sussmann and V. I. Utkin, eds. Nonlinear and optimal control theory. Springer, London.
20. Liu, J., W. Luo, X. Yang, and L. Wu. 2016. Robust model-based fault diagnosis for PEM fuel cell air-feed system. IEEE Trans. Industr. Electron. 63:3261–3270.
21. Liu, J., Y. Yin, W. Luo, S. Vazquez, L. G. Franquelo, and L. Wu. 2017. Sliding mode control of a three-phase AC/DC voltage source converter under unknown load conditions: industry applications. IEEE Transactions on Systems, Man, and Cybernetics: Systems.
22. Liu, J., S. Vazquez, L. Wu, A. Marquez, H. Gao, and L. G. Franquelo. 2017. Extended state observer-based

sliding-mode control for three-phase power converters. IEEE Trans. Industr. Electron. 64:22–31.
23. Harmouche, M., I. Matraji, S. Laghrouche, and M. El-Bagdouri. 2012. Homogeneous higher order sliding mode control for PEM fuel cell. 12th International Workshop on Variable Structure Systems.
24. Matraji, I., S. Laghrouche, and M. Wack. 2012. Pressure control in a PEM fuel cell via second order sliding mode. Int. J. Hydrogen Energy 37:16104–16116.
25. Rakhtala, S. M., A. R. Noei, R. Ghaderi, and E. Usai. 2015. Control of oxygen excess ratio in a PEM fuel cell system using high-order sliding-mode controller and observer. Turk. J. Electr. Eng. Co. 23:255–278.
26. Talj, R. J., D. Hissel, R. Ortega, M. Becherif, and M. Hilairet. 2010. Experimental validation of a PEM fuel-cell reduced-order model and a moto-compressor higher order sliding-mode control. IEEE Trans. Industr. Electron. 57:1906–1913.
27. Kunusch, C., P. F. Puleston, M. A. Mayosky, and A. Davila. 2010. Efficiency optimisation of an experimental PEM fuel cell system via super twisting control. 11th International Workshop on Variable Structure Systems (VSS).
28. Matraji, I., F. S. Ahmed, S. Laghrouche, and M. Wack. 2012. Extremum seeking control for net power output maximization of a PEM fuel cell using second order sliding mode. 12th International Workshop on Variable Structure Systems (VSS).
29. Matraji, I., J. Liu, S. Laghrouche, and M. Wack. 2012. Adaptive second order sliding mode control of PEM fuel cell air feed system. IEEE 51st IEEE Conference on Decision and Control (CDC).
30. Mefoued, S. 2015. A second order sliding mode control and a neural network to drive a knee joint actuated orthosis. Neurocomputing 155:71–79.
31. RakhtAla, S. M., M. Yasoubi, and H. HosseinNia. 2017. Design of second order sliding mode and sliding mode algorithms: a practical insight to DC-DC buck converter. IEEE/CAA J. Automat. Sin. 4:483–497.
32. Evangelista, C., P. Puleston, and F. Valenciaga. 2010. Variable gains super-twisting control for wind energy conversion optimization. 11th International Workshop on Variable Structure Systems (VSS).
33. Evangelista, C., P. Puleston, F. Valenciaga, and L. M. Fridman. 2013. Lyapunov-designed super-twisting sliding mode control for wind energy conversion optimization. IEEE Trans. Industr. Electron. 60:538–545.
34. Gonzalez, T., J. Moreno, and L. Fridman. 2012. Variable gain super-twisting sliding mode control. IEEE Trans. Autom. Control 57:2100–2105.
35. Moreno, J., and M. Osorio. 2012. Strict Lyapunov functions for the super-twisting algorithm. IEEE Trans. Autom. Control 57:1035–1040.
36. Moreno, J. A. 2012. Lyapunov approach for analysis and design of second order sliding mode algorithms. Pp. 113–149 *in* L. Fridman, J. Moreno and R. Iriarte, eds. Sliding modes after the first decade of the 21st century. Springer, London.
37. Shtessel, Y., M. Taleb, and F. Plestan. 2012. A novel adaptive-gain supertwisting sliding mode controller: methodology and application. Automatica 48:759–769.
38. Utkin, V. I., and A. S. Poznyak. 2013. Adaptive sliding mode control with application to super-twist algorithm: equivalent control method. Automatica 49:39–47.
39. Segura, F., and J. M. Andújar. 2012. Power management based on sliding control applied to fuel cell systems: a further step towards the hybrid control concept. Appl. Energy 99:213–225.
40. Park, G., and Z. Gajic. 2012. Sliding mode control of a linearized polymer electrolyte membrane fuel cell model. J. Power Sources 212:226–232.
41. Rakhtala, S. M., A. R. Noei, R. Ghaderi, and E. Usai. 2014. Design of finite-time high-order sliding mode state observer: a practical insight to PEM fuel cell system. J. Process Control 24:203–224.
42. Garcia-Gabin, W., F. Dorado, and C. Bordons. 2010. Real-time implementation of a sliding mode controller for air supply on a PEM fuel cell. J. Process Control 20:325–336.
43. Levant, A. 1993. Sliding order and sliding accuracy in sliding mode control. Int. J. Control 58:1247–1263.
44. Moreno, J. A., and M. Osorio. 2008. A Lyapunov approach to second-order sliding mode controllers and observers. 47th IEEE Conference on Decision and Control.
45. Evangelista, C., P. Puleston, and C. Kunusch. 2014. Feasibility study of variable gain Super-Twisting control in fuel cells based systems. 13th International Workshop on Variable Structure Systems (VSS).

Appendix

Table A1. Value of parameters of the PEMFC [41].

Parameter	Symbol	SI units	Value
Atmospheric pressure	P_{atm}	Pa	101.325
Saturation pressure in ambient temperature	$P_{sat,atm}$	Pa	3.1404×10^3
Saturation pressure in stack temperature	$P_{sat,Tst}$	Pa	4.0943×10^4
Average ambient air relative humidity	$\varnothing_{atm}$	–	0.5
Relative humidity in cathode inlet	$\phi_{ca,in}^{des}$	–	1
Atmospheric temperature	T_{atm}	K	298.15
Air-specific heat ratio	γ	–	1.4
Air density	C_p	J/kg/K	1004
Universal gas constant	R	J/mol/K	8.31451
Air density	ρ_a	kg/m^3	1.23
Air gas constant	R_a	J/mol/K	286.9
Oxygen gas constant	R_{O_2}	J/kg/K	259.8
Nitrogen gas constant	R_{N_2}	J/kg/K	296.8
Vapor gas constant	R_v	J/kg/K	461.5
Molar mass of air	Ma	kg/mol	28.97×10^{-3}
Molar mass of oxygen	M_{O_2}	kg/mol	30×10^{-3}
Molar mass of nitrogen	M_{N_2}	kg/mol	28×10^{-3}
Molar mass of vapor	M_v	kg/mol	18.02×10^{-3}
Maximum molar mass of vapor in cathode	$m_{v,ca,max}$	kg/mol	0.002889
Faraday's constant	F	C/mol	96,487
Temperature of the stack	T_{st}	K	353

Table A2. Parameters affecting modeling of the PEMFC [41].

Parameter	Symbol	SI units	Value
Motor constant	K_t	N m/A	0.0153
Motor constant	R_{cm}	ohm	0.82
Motor constant	K_v	V/(rad/sec)	0.0153
Compressor efficiency	η_{cp}	–	0.8
Compressor motor mechanical efficiency	η_{cp}	–	0.98
Number of cells in fuel cell stack	n	–	381
Fuel cell active area	A_{fc}	m^2	280×10^{-4}
Supply manifold volume	V_{sm}	m^3	0.02
Single stack cathode volume	V_{ca}	m^3	0.005
Return manifold volume	V_{rm}	m^3	0.005
Supply manifold outlet orifice constant	$K_{sm,out}$	kg/sec/Pa	0.3629×10^{-5}
Cathode outlet orifice constant	$K_{ca,out}$	kg/sec/Pa	0.2177×10^{-5}
Compressor diameter	d_c	m	0.2286
Oxygen mole fraction at cathode inlet	$y_{O_2,in}$	–	0.21

Table A3. Polynomial coefficients of equations [41].

B_{00}	4.83×10^{-5}kg/sec
B_{10}	-5.42×10^{-5}kg/sec^2
B_{20}	8.79×10^{-6}kg/sec^3
B_{01}	3.49×10^{-7}kg/sec^2/bar
B_{11}	3.55×10^{-13}kg/sec
B_{02}	-4.11×10^{-10}kg/sec/bar